Dynamic Roles of Arginine Residues 82 and 92 of *Escherichia coli* 6-Hydroxymethyl-7,8-dihydropterin Pyrophosphokinase: Crystallographic Studies[†,‡]

Jaroslaw Blaszczyk,[§] Yue Li,[||] Genbin Shi,[||] Honggao Yan,[||] and Xinhua Ji*[,§]

Macromolecular Crystallography Laboratory, National Cancer Institute, Frederick, Maryland 21702, and Department of Biochemistry, Michigan State University, East Lansing, Michigan 48824

Received September 4, 2002; Revised Manuscript Received December 6, 2002

ABSTRACT: 6-Hydroxymethyl-7,8-dihydropterin pyrophosphokinase (HPPK) catalyzes the pyrophosphoryl transfer from ATP to 6-hydroxymethyl-7,8-dihydropterin (HP), the first reaction in the folate biosynthetic pathway. Arginine residues 82 and 92, strictly conserved in 35 HPPK sequences, play dynamic roles in the catalytic cycle of the enzyme. At 0.89-Å resolution, two distinct conformations are observed for each of the two residues in the crystal structure of the wild-type HPPK in complex with two HP variants, two Mg^{2+} ions, and an ATP analogue. Structural information suggests that R92 first binds to the α-phosphate group of ATP and then shifts to interact with the β-phosphate as R82, which initially does not bind to ATP, moves in and binds to α-phosphate when the pyrophosphoryl transfer is about to occur. The dynamic roles of R82 and R92 are further elucidated by five more crystal structures of two mutant proteins, R82A and R92A, with and without bound ligands. Two oxidized forms of HP are observed with an occupancy ratio of 0.50:0.50 in the 0.89-Å structure. The oxidation of HP has significant impact on its binding to the protein as well as the conformation of nearby residue W89.

6-Hydroxymethyl-7,8-dihydropterin pyrophosphokinase (HPPK)[1] catalyzes the pyrophosphoryl transfer from ATP to 6-hydroxymethyl-7,8-dihydropterin (HP, Figure 1), the first reaction in the folate biosynthetic pathway (*1*). Folate cofactors are essential for life (*2*). Mammals have an active transport system for deriving folates from their diet. In contrast, most microorganisms must synthesize folates de novo because they lack the active transport system. Therefore, the folate pathway is an ideal target for developing antimicrobial agents (*3*−*7*). Inhibitors of two enzymes of the pathway, dihydropteroate synthase (*8*) and dihydrofolate reductase (*9*), are currently used as antibiotics. HPPK is not the target for any existing antibiotic and therefore is an ideal target for development of novel antimicrobial agents. As a small, thermostable, and monomeric protein, *Escherichia coli* HPPK is also an excellent model system for studying the mechanisms of pyrophosphoryl transfer, about which little is known.

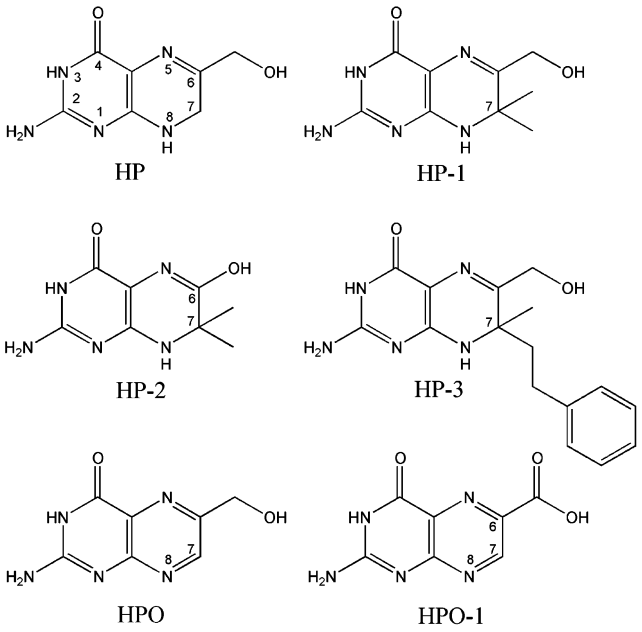

FIGURE 1: Structures of 6-hydroxymethyl-7,8-dihydropterin (HP), 6-hydroxymethylpterin (HPO), and their derivatives HP-1, HP-2, HP-3, and HPO-1.

Three-dimensional structures in various liganded states have been reported, including apo-HPPK (PDB 1hka, ref *10*); HPPK in complex with HP-2 (an HP analogue, Figure 1) (PDB 1cbk, ref *11*); with Mg^{2+} and ADP (PDB 1eqm, ref *12*); with Mg^{2+} and β,γ-methyleneadenosine 5′-triphosphate (AMPPCP, an ATP analog) (PDB 1eq0, ref *12*); with HP-3 (an HP analogue, Figure 1), two Mg^{2+} ions, and ATP (PDB 1dy3, ref *13*); with HP, two Mg^{2+} ions, and α,β-methyleneadenosine 5′-triphosphate (AMPCPP, an ATP analog) (PDB

[†] This work was supported in part by NIH Grant GM51901 (H.Y.).

[‡] The coordinates and structure factors have been deposited in the Protein Data Bank with the accession codes 1f9y for HPPK·HPO/HPO-1·MgAMPCPP, 1hq2 for HPPK(R82A)·HP·MgAMPCPP, 1f9h for HPPK(R92A)·HP·MgAMPCPP, 1im6 for apo-HPPK(R82A), 1kbr for apo-HPPK(R92A), and 1g4c for HPPK(R92A)·Mg.

* Corresponding author. Phone: (301) 846-5035. Fax: (301) 846-6073. E-mail: jix@ncifcrf.gov.

[§] National Cancer Institute.

[||] Michigan State University.

[1] Abbreviations: AMPCPP, α,β-methyleneadenosine 5′-triphosphate; AMPPCP, β,γ-methyleneadenosine 5′-triphosphate; BM, binding mode; HP, 6-hydroxymethyl-7,8-dihydropterin; HPPK, 6-hydroxymethyl-7,8-dihydropterin pyrophosphokinase; HPO, 6-hydroxymethylpterin; HPO-1, 6-carboxylpterin; MR, molecular replacement; PDB, the Protein Data Bank; rmsd, root-mean-square deviation.

10.1021/bi0267994 CCC: $25.00
Published on Web 01/21/2003

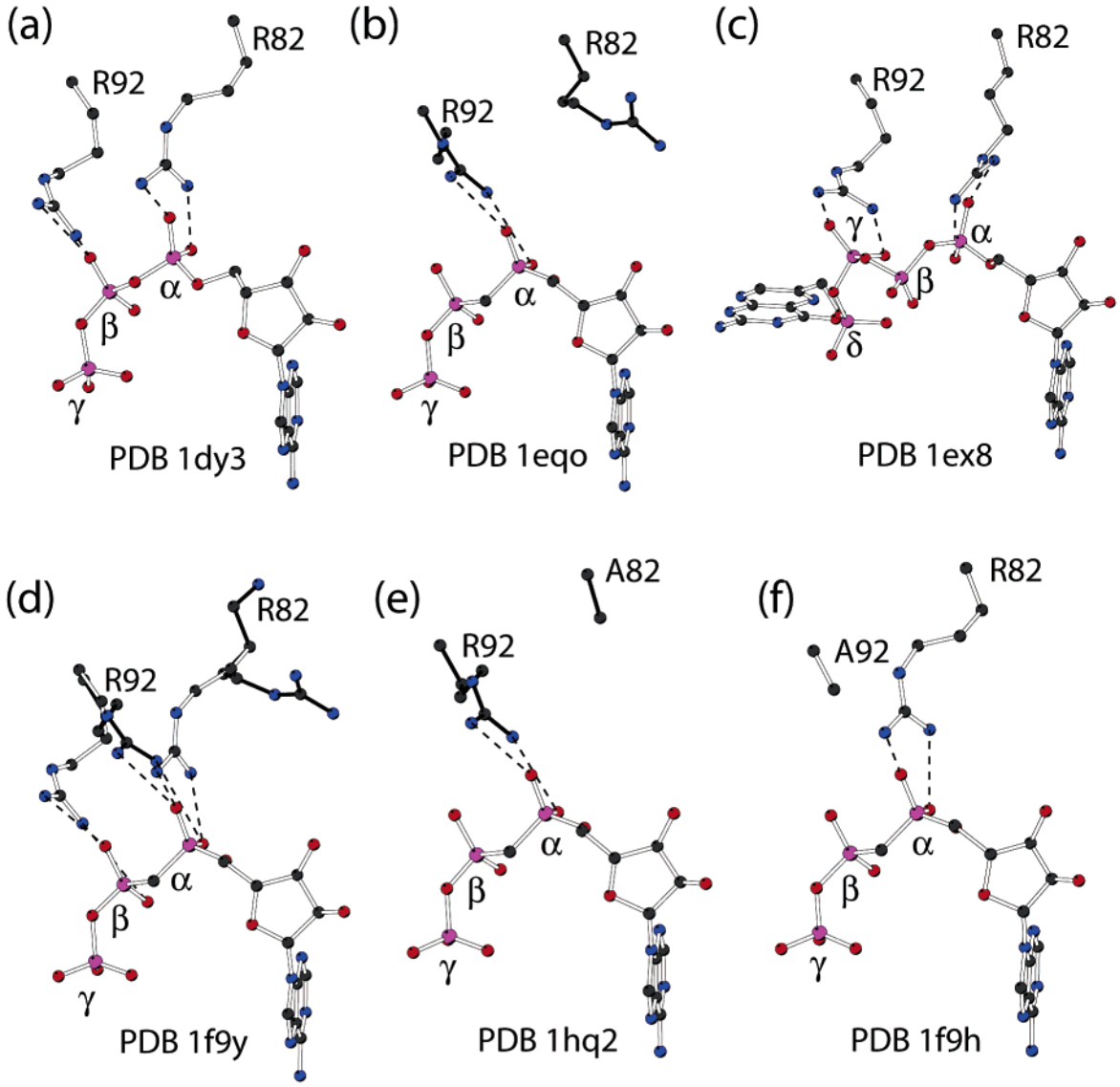

FIGURE 2: Conformations of R82 and R92 as observed in the ternary complexes of HPPK. (a) HPPK·HP-3·MgATP (PDB 1dy3, ref *13*); (b) HPPK·HP·MgAMPCPP (PDB 1eqo, ref *14*); (c) HPPK·MgHP$_4$A (PDB 1ex8, ref *15*); (d) HPPK·HPO/HPO-1·MgAMPCPP (PDB 1f9y, this paper); (e) R82A·HP·MgAMPCPP (PDB 1hq2, this paper); and (f) R92A·HP·MgAMPCPP (PDB 1f9h, this paper). Open bonds of R82 and R92 indicate binding mode I, whereas filled bonds are for binding mode II (see text for details).

1eqo, ref *14*); and with two Mg^{2+} ions and P^1-(6-hydroxymethylpterin)-P^4-(5′-adenosyl)tetraphosphate (HP$_4$A, a bisubstrate analog) (PDB 1ex8, ref *15*). These structures are critical both for drug design and for elucidation of the catalytic mechanism. We have summarized the structure-and-function relationship of 26 residues, among which 13 are conserved in 11 HPPK sequences (*14*). This study is focused on two arginine residues, 82 and 92, which are strictly conserved in 35 HPPK proteins sequenced to date.

The side chains of R82 and R92 appear to be parallel in all known structures (see Figure 2 for examples). Nonetheless, two distinct conformations have been observed for these two side chains. In the crystal structure of HPPK·HP-3·MgATP (1dy3, ref *13*), the guanidinium group of R82 interacts with α-phosphate, and that of R92 interacts with *β*-phosphate (Figure 2a). In the HPPK·HP·MgAMPCPP complex (1eqo, ref *14*), however, R92 interacts with α-phosphate, and R82 does not interact with ATP (Figure 2b). Similar to the former (Figure 2a), both R82 and R92 interact with phosphate groups of the inhibitor (Figure 2c) in the HPPK·Mg HP$_4$A complex (PDB 1ex8, ref *15*). Note that the pyrophosphoryl transfer reaction requires the cleavage of the ester bond between the α- and *β*-phosphate groups. Therefore, the former (Figure 2a) is most likely the catalytic binding mode (BM) of R82 and R92, which anchors both α- and *β*-phosphates for the reaction to occur. For the ease of discussion, the two sets of R82/R92 conformations are thereafter referred to as BM I (Figure 2a) and BM II (Figure 2b). To elucidate the functional roles of R82 and R92, we have carried out site-directed mutagenesis, biochemical (see the companion paper for details), and crystallographic studies. Here, we present six crystal structures of either the wild-type protein or the R82A and R92A mutants with and without bound ligands at the resolutions ranging from 0.89 to 1.74 Å.

In the 0.89-Å structure of HPPK complexed with 6-hydroxymethylpterin (HPO)/6-carboxylpterin (HPO-1), two Mg^{2+} ions, and AMPCPP, we observed both BM I and BM II for arginine residues 82 and 92 (Figure 2d), suggesting

Table 1: Protein and Reservoir Solutions for the Crystallization of HPPK Proteins

	1[a]	2	3	4	5	6
			Protein Solution			
HPPK proteins	wild type	R82A	R92A	R82A	R92A	R92A
protein (mg/mL)	9	9	9	11	9	9
AMPCPP (mM)	15	25	25			
HP (mM)	25	15	15			
$MgCl_2$ (mM)	50	50	50			
Tris-HCl [mM (pH)]	10 (8.0)	10 (8.0)	10 (8.0)	10 (8.0)	10 (8.0)	10 (8.0)
			Reservoir Solution			
PEG 4000 [%(w/v)]	30	25	27	27	30	30
CH_3·$COONH_4$ (mM)	200	170	180			
CH_3·COONa (mM)				180	200	200
$MgCl_2$ (mM)				50		50
NaCl (mM)					100	
H·COONa (mM)				700		
glycerol [%(v/v)]	2	10	10			
Tris-HCl [mM (pH)]				90 (8.4)	100 (8.5)	100 (8.5)
CH_3·COONa [mM (pH)]	100 (4.6)	100 (4.6)	90 (4.6)			
			Crystals			
shape	needle	needle	needle	plate	plate	plate
dimension ($\times 10^{-2}$ mm)	15 × 15 × 35	7 × 7 × 20	.5 × .5 × 10	1 × 1 × 25	.5 × 30 × 30	.3 × 15 × 20

[a] 1, HPPK·HPO/HPO-1·MgAMPCPP; 2, R82A·HP·MgAMPCPP; 3, R92A·HP·MgAMPCPP; 4, apo-R82A; 5, apo-R92A; and 6, R92A·Mg.

that R82 and R92 play dynamic roles in the catalytic cycle of HPPK.

EXPERIMENTAL PROCEDURES

Protein Expression, Purification, and Crystallization. Wild-type HPPK and point mutants R82A and R92A were expressed and purified according to the protocol established for the wild-type protein (*16*). The crystallization condition for HPPK·HPO/HPO-1·MgAMPCPP (Table 1) was similar to that for HPPK·HP·MgAMPCPP (*14*). The important difference, which resulted in the oxidation of HP, was the incubation time before setting up crystallization experiments and the time for the crystals to appear. For HPPK·HP·MgAMPCPP (*14*), the protein was incubated with substrate/inhibitor for ~0.5 h before setting up the vapor diffusion experiments, and the crystals appeared overnight. For the HPO/HPO-1 complex, the protein was incubated with HP and MgAMPCPP for ~5 h at 19 ± 1 °C and then overnight at 4 ± 1 °C prior to setting up the crystallization drops. The crystals appeared in approximately one week and reached the dimensions shown in Table 1 in four weeks.

All crystals of HPPK mutant proteins were grown at 19 ± 1 °C with the hanging-drop vapor-diffusion technique. The drops contained equal volumes of protein stock and reservoir solutions (Table 1). Crystals of apo-R82A appeared in 3 days and after two more weeks reached the size suitable for data collection (Table 1). Crystals of apo-R92A and R92A·Mg appeared in a few minutes and reached the final size in 4−5 days. Crystals of R82A·HP·MgAMPCPP appeared in 24 h and grew to the final dimensions (Table 1) in two more days. Small crystals of R92A·HP·MgAMPCPP appeared in 3 days and stopped growing thereafter.

Data Collection and Processing, Structure Solution and Refinement. X-ray diffraction data for all six structures were collected at cryogenic temperature (100 K), with an ADSC Quantum-4 CCD detector mounted at the synchrotron beamline X9B of the National Synchrotron Light Source, Brookhaven National Laboratory. Data processing was carried out with the HKL2000 program suite (*17*). Details of data collection and processing are summarized in Table 2. All crystals diffracted to high resolution. The crystals of three ternary complexes belong to space group *C*2 and their unit cell parameters are similar to those of HPPK·HP·MgAMPCPP (*14*). The crystals of two ligand-free proteins belong to space group $P2_1$, and their unit cell parameters are similar to those of apo-HPPK (*10*). Although the crystal of R92A·Mg belongs to space group $P2_1$, the unit cell dimensions are different from those of apo-HPPK (*10*).

Five out of six structures were determined using the difference Fourier technique, and the structure of R92A·Mg was solved using the molecular replacement (MR) program AmoRe (*18*). See Table 2 for the starting model for difference Fourier synthesis and search model for MR. All ligands and solvent molecules were removed from the starting models. The initial refinement was carried out with simulated annealing methods using CNS (*19*), followed by the least-squares refinement using SHELXL-97 (*20*). Model building and rebuilding were carried out using O (*21*).

For apo-R82A, apo-R92A, and R92A·Mg, isotropic thermal parameters for all non-hydrogen atoms were refined individually. For the three ternary complexes, ordered atoms were refined with anisotropic temperature factors, whereas disordered atoms were refined with isotropic temperature factors. The hydrogen atoms of anisotropically refined atoms were built geometrically at their idealized positions with assigned isotropic thermal parameters equal to 1.2× equivalent isotropic thermal parameters of their parent atoms. Positional parameters of ligands and ions were refined without geometric restraints.

Water molecules were identified in the difference Fourier map as positive peaks above 3σ. The presence of Mg^{2+} and Cl^- ions was verified by refining the structure with assumed atomic identity and observing the behavior of their temperature factors. The geometry of refined structures was assessed using PROCHECK (*22*). The details of refinement and statistics of final structures are summarized in Table 2.

Table 2: Summary of Structure Solution and Refinement of HPPK Structures

	1[a]	2	3	4	5	6
resolution (Å)	0.89	1.25	1.50	1.74	1.55	1.65
measured reflections	451 128	126 338	78 292	50 062	81 783	88 579
unique reflections	100 866	39 345	22 905	14 272	19 262	32 443
overall completeness (%)	99.6	99.3	93.1	95.9	96.3	98.7
last shell completeness (%)	75.6	99.0	94.2	93.9	92.5	98.0
overall R_{merge}[b]	0.043	0.092	0.100	0.108	0.093	0.071
last shell R_{merge}	0.581	0.571	0.449	0.403	0.510	0.491
overall I/σ	31.0	12.3	12.1	11.4	14.6	13.9
last shell I/σ	1.7	1.7	2.2	2.2	1.8	2.0
space group	*C*2	*C*2	*C*2	$P2_1$	$P2_1$	$P2_1$
unit cell parameters						
a (Å)	73.466	73.372	73.612	36.106	36.340	42.351
b (Å)	37.910	37.843	37.783	47.178	46.943	47.210
c (Å)	57.849	58.018	57.970	43.816	42.907	71.306
β (deg)	117.18	117.18	117.04	109.44	110.49	105.61
no. molecules/asymmetric unit	1	1	1	1	1	2
solvent content (%)	33.4	33.5	33.5	35.1	35.0	33.4
Matthews coefficient ($Å^3$/Da)	1.92	1.92	1.92	1.97	1.96	1.92

starting model	PDB 1eqo[c]	PDB 1eqo[c]	PDB 1eqo[c]	PDB 1hka[c]	PDB 1im6[c]	PDB 1hka[d]
no. data in refinement: $2\sigma(I)$/all	77 218/95 772	26 465/37 252	16 291/21 774	10 417/13 121	13 591/18 109	22 944/30 749
no. data for R_{free}: $2\sigma(I)$/all	4145/5090	1338/1932	811/1084	577/655	708/944	1241/1659
no. least-squares parameters	15 215	14 475	14 342	6187	5140	10 355
no. residues/(non-H) atoms	158/1345	158/1287	158/1275	158/1261	158/1277	316/2532
no. heterogen atoms	61	64	48	1	1	6
no. water oxygen atoms	416	333	412	279	230	425
final R_{free}: $2\sigma(I)$/all	0.118/0.133	0.132/0.172	0.118/0.151	0.207/0.216	0.183/0.208	0.196/0.236
final *R*: $2\sigma(I)$/all	0.097/0.112	0.097/0.134	0.084/0.111	0.161/0.187	0.160/0.192	0.162/0.205
rmsd (Å)						
bond lengths	0.021	0.011	0.009	0.006	0.008	0.011
angle distances	0.036	0.027	0.027	0.021	0.025	0.026
estimated coordinate error (Å)	0.063	0.10	0.07	0.17	0.16	0.15
Ramachandran plot (%):						
most favored regions	97.1	96.3	97.1	97.1	95.6	94.5
disallowed regions	0	0	0	0	0	0

[a] 1, HPPK·HPO/HPO-1·MgAMPCPP; 2, R82A·HP·MgAMPCPP; 3, R92A·HP·MgAMPCPP; 4, apo-R82A; 5, apo-R92A; and 6, R92A·Mg. [b] $R_{merge} = \sum|(I - \langle I\rangle)|/\sum(I)$, where *I* is the observed intensity. [c] Difference Fourier. [d] Molecular replacement solution with a correlation coefficient of 0.66 and crystallographic *R* factor of 0.42 for X-ray data within the resolution range of 10.0−4.0 Å.

RESULTS AND DISCUSSION

Quality of the Structures. At 0.89-Å resolution, the identity of atoms is clearly indicated by the size of their electron densities (for example, see Figure 3). The crystal structure of HPPK·HPO/HPO-1·MgAMPCPP unambiguously revealed the identities of HPO and HPO-1 (Figure 1) with an occupancy ratio of 0.50:0.50 (Figure 3b). Residues P43, V58, S63, E68, L78, Q79, R82, V83, E87, W89, R92, D103, L111, M142, and H148 exhibit two conformations of equal probability; the electron density for W89, R82, and R92 is shown in Figure 3. Two side chain conformations were found for S13 and L135 with an occupancy ratio of 0.66:0.33. Three conformations were found for E67 with an occupancy ratio of 0.50:0.25:0.25. Multi-conformations of side chains have also been revealed in the other five structures.

All protein atoms, ligands, and solvent molecules have well-defined electron density, with only a few exceptions in ligand-free structures. In apo-R82A, incomplete density was observed for the side chains of surface residues Q48, D49, and E67, among which Q48 and D49 are located in the flexible loop 2. In apo-R92A, weak density was observed for residues 46−50 of loop 2, 86−90 of loop 3, and solvent-exposed K154 near the C-terminus. In R92A·Mg, weak density was observed for side-chains of Q48, K85, and R88 of molecule A.

The electron density of R92A·Mg revealed the presence of two Mg^{2+} ions bound to D95 and D97 of molecule B, one of the two crystallographically independent molecules (Table 2). Both Mg^{2+} ions are six-coordinated. The side chain of E16 from molecule A is coordinated with one of the two Mg^{2+} ions. In all six structures, a Cl^- ion has been found near the amide nitrogen of E139, as observed in the structure of HPPK·HP·MgAMPCPP (PDB 1eqo, ref *14*).

Structure and Function of R82 and R92. The 0.89-Å structure of HPPK·HPO/HPO-1·MgAMPCPP reveals two conformations for both R82 and R92 (Figures 2d and 3a). Previous observations have demonstrated that the two side chains are always approximately parallel to each other (Figure 2a−c) and assume two sets of distinct conformations, BM I (Figure 2a) and BM II (Figure 2b). We observed both BMs for R82 and R92 in the crystal structure of HPPK·HPO/HPO-1·MgAMPCPP, suggesting that these two residues play dynamic roles in HPPK catalysis.

For BM I, the guanidinium group of R92 binds to the β-phosphate of ATP and that of R82 binds to the α-phosphate of ATP (Figure 2a); whereas for BM II, the guanidinium group of R92 binds to the α-phosphate of ATP and that of R82 is not involved in direct interaction with ATP (Figure 2b). We further discovered that no matter which of the two arginine side chains is absent, the existing arginine always interacts with the α-phosphate group of ATP by assuming a

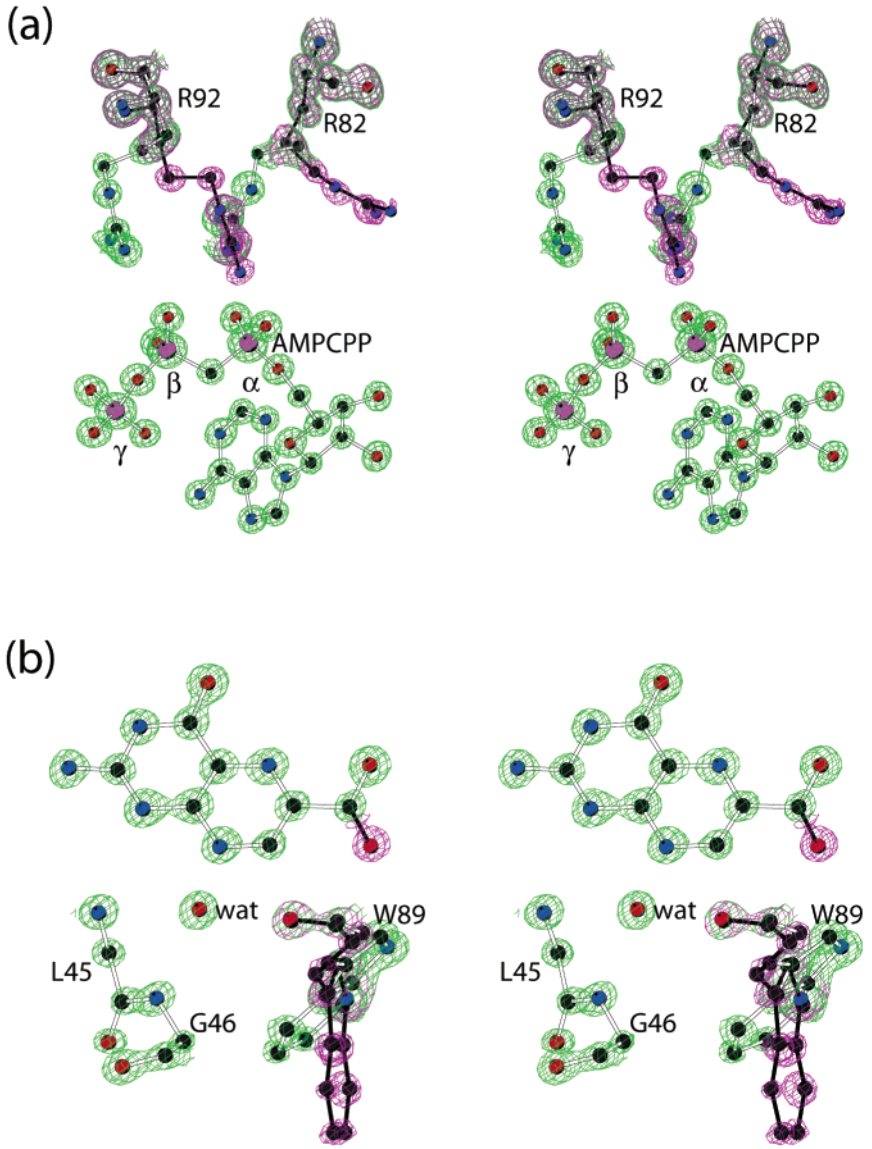

FIGURE 3: Stereoviews showing the representative $2F_o - F_c$ electron density for the 0.89-Å structure of HPPK·HPO/HPO-1·MgAMPCPP contoured at 3σ for ordered residues/substrates and at 1.5σ for disordered residues. (a) Electron densities for R82, R92, and AMPCPP. (b) Electron density for L45, G46, W89, and HPO/HPO-1.

conformation corresponding to either BM II (Figure 2e) or BM I (Figure 2f), suggesting that for ATP binding, the two arginines have comparable significance. Because the pyrophosphoryl transfer reaction involves the breakage of the ester bond between the α- and the β-phosphate groups, we suggest that R92 is essential for catalysis by playing dual roles, ATP binding and ester bond breaking. It binds to the α-phosphate group of ATP (Figure 2b) and shifts to interact with β-phosphate as R82 binds to α-phosphate (Figure 2a) when the pyrophosphoryl transfer is about to occur. This is in agreement with our biochemical data. The substitution of R82 with alanine caused a decrease in the rate constant for the chemical step by a factor of ~380, whereas the substitution of R92 with alanine caused a decrease in the rate constant for the chemical step by a factor of $\sim 3.5 \times 10^4$ (see companion paper for details).

Point Mutations R82A and R92A and their Structural Impact. Figure 4a shows the superposition of the structures of apo-HPPK (*10*), apo-R82A (this paper), and apo-R92A (this paper). All three proteins belong to space group $P2_1$ with very similar unit cell dimensions (Table 2). Superposition of the three Cα traces reveals that the two mutant structures are quite similar with an rmsd of 0.25 Å, but the two mutant structures are rather different from the wild type in several regions (Figure 4a). First, loop 1 of apo-HPPK has two conformations, whereas it assumes only one conformation in the mutants. Second, significant conformational differences are observed for loop 2, in which the maximal Cα atom displacement reaches 5.0 Å for P47. Third and dramatically, the conformation of loop 3 in both mutant proteins is very different from that in the wild type, where the largest Cα atom displacement reaches 9.5 Å for R84. Fourth and interestingly, the C-terminal region of the two mutant proteins is very different from the wild type; the maximal Cα shift in this area reaches ~4.5 Å for D153. Fifth, although R82 and R92 side chains point to the opposite direction of the active center in all three proteins, their positions in the mutants are rather different from those in the wild-type protein (Figure 4a).

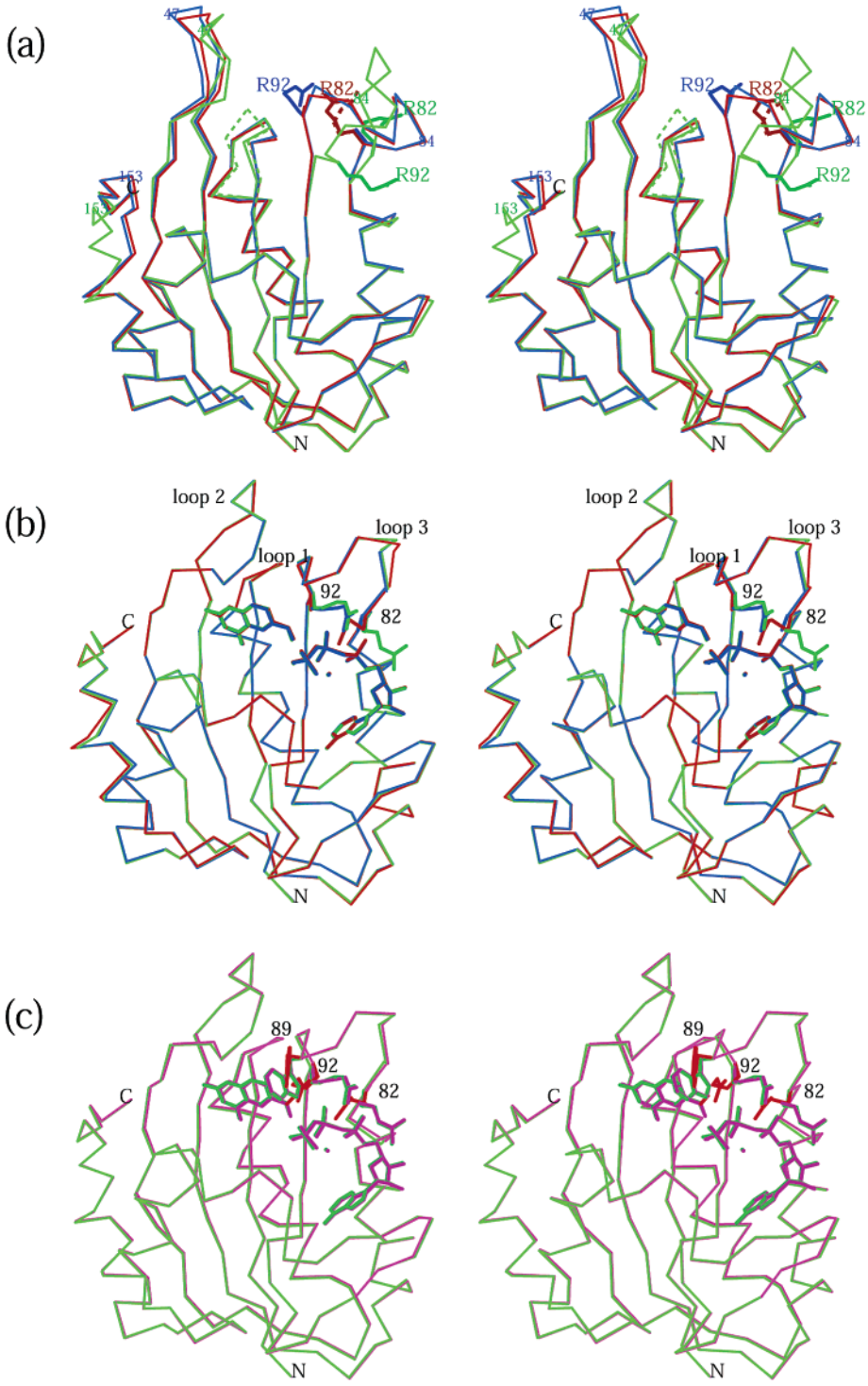

FIGURE 4: Stereoviews illustrating the superposition of Cα traces, ligand molecules, and side chains of R82 and R92 in (a) apo-HPPK (green, ref *10*), apo-R82A (blue, this paper), and apo-R92A (orange, this paper); (b) HPPK·HP·MgAMPCPP (in green, PDB 1eqo, ref *14*), R82A·HP·MgAMPCPP (blue, this paper), and R92A·HP·MgAMPCPP (orange, this paper); and (c) HPPK·HP·MgAMPCPP (green, PDB 1eqo, ref *14*) and HPPK·HPO/HPO-1·MgAMPCPP (magenta, this paper).

While significant differences exist in the apo-structures of the wild-type and the mutant proteins, no significant difference is found in the overall structure of their ternary complexes. Figure 4b depicts the superposition of three ternary complex structures, including HPPK·HP·MgAMPCPP (*14*), R82A·HP·MgAMPCPP (this paper), and R92A·HP·MgAMPCPP (this paper). The Mg^{2+} ions, the HP and AMPCPP molecules, and the Cα traces superimpose very well between the three structures; the rmsd between the wild type and any mutant protein is 0.08 Å for all 158 Cα positions (Figure 4b). The largest shift of main chain atoms is ~0.5 Å between HPPK·HP·MgAMPCPP (*14*) and R82A·HP·MgAMPCPP (this paper) and ~1.4 Å between HPPK·HP·MgAMPCPP (*14*) and R92A·HP·MgAMPCPP (this paper). All the interactions between the protein and the ligands (Mg^{2+} ions and the HP and AMPCPP molecules) are maintained in the structure of R82A·HP·MgAMPCPP. In the case of R92A, the loss of the hydrogen bonds between

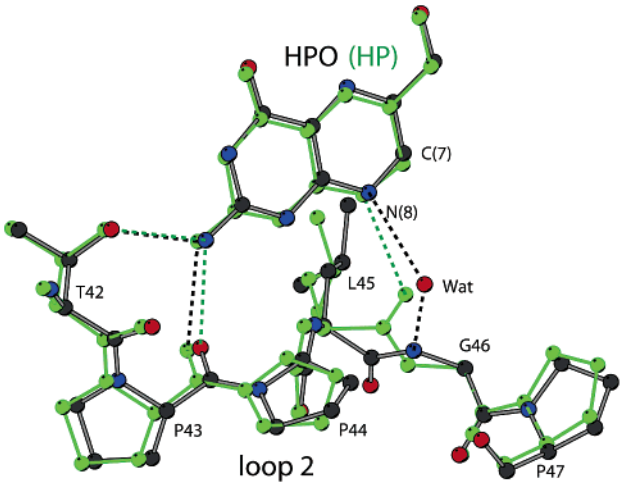

FIGURE 5: Superposition of HPO and loop 2 residues in HPPK·HPO/HPO-1·MgAMPCPP (in atomic color: carbon black, nitrogen blue, and oxygen red) with HP and corresponding residues in HPPK·HP·MgAMPCPP (green, PDB 1eqo, ref *14*). Hydrogen bonds are shown as dashed lines.

the guanidinium group of R92 and AMPCPP is expected, which is partially compensated by the guanidinium groups of R82 and R84. The guanidinium group of R82 forms one hydrogen bond and that of R84 two hydrogen bonds with the α-phosphate of AMPCPP. In HPPK·HP·MgAMPCPP, the guanidinium group of R82 has no direct interaction with AMPCPP and that of R84 forms one hydrogen bond with the α-phosphate and one hydrogen bond with the 3′-hydroxyl group of AMPCPP. All the other interactions between the protein and the ligands in R92A·HP·MgAMPCPP (this paper) are the same as those found in HPPK·HP·MgAMPCPP (*14*). The structures of the ternary complexes of the two mutants suggest that the dramatic decreases in the catalytic power of HPPK caused by the mutations are due to the removal of the specific interactions rather than conformational perturbations.

Structure and Structural Impact of Oxidized Forms of HP. HPO and HPO-1 are the oxidized forms of HP (Figure 1). The oxidation occurred during the incubation before crystallization experiments (see Experimental Procedures). In HP,

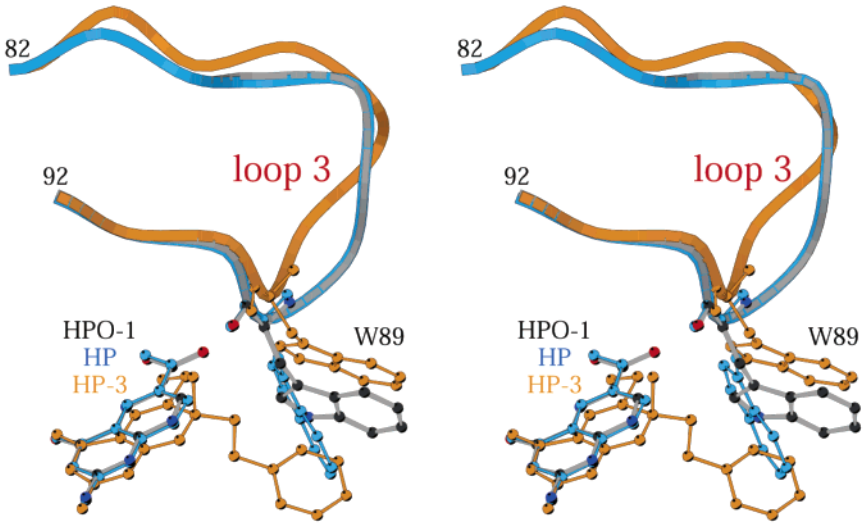

FIGURE 6: Stereoview depicting the superposition of HPO-1/W89 in HPPK·HPO/HPO-1·MgAMPCPP (in atomic color: carbon black, nitrogen blue, and oxygen red, this paper) with HP/W89 in HPPK·HP·MgAMPCPP (cyan, PDB 1eqo, ref *14*) and HP-3/W89 in HPPK·HP-3·MgATP (yellow, PDB 1dy3, ref *13*). The HPO/W89 pair in HPPK·HPO/HPO-1·MgAMPCPP (this paper) has identical conformation with the HP/W89 pair in HPPK·HP·MgAMPCPP (cyan, ref *14*) and is not shown for clarity.

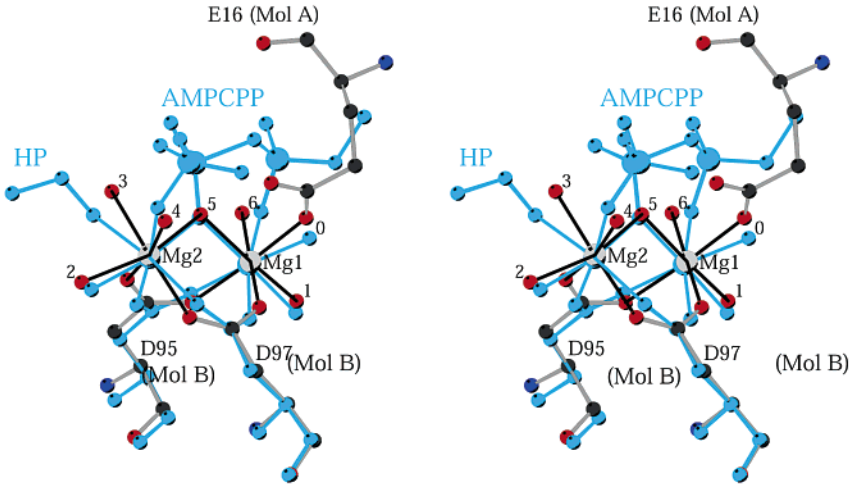

FIGURE 7: Stereoview showing the Mg^{2+} coordination as observed in R92A·Mg (in atomic color with black carbon, blue nitrogen, and red oxygen, this paper) and in HPPK·HP·MgAMPCPP (cyan, PDB 1eqo, ref *14*). Water molecules involved in Mg^{2+} coordination are identified as 0−6.

the bond distance for the single bond between C7 and N8 is 1.41 Å (*14*). In HPO, however, this distance becomes 1.36 Å (this paper), suggesting the formation of the double bond between C7 and N8 is due to removal of the hydrogen atom on N8 and one of the two hydrogen atoms on C7 (Figure 1). Difference density revealed a positive peak above 3σ, located 1.28 Å away from the carbon atom of the $-CH_2OH$ moiety, suggesting that further oxidation of $-CH_2OH$ results in the formation of a $-$COOH group (HPO-1, Figure 1). The occupancy ratio of HPO/HPO-1 is 0.50:0.50 as determined by nonrestrained least-squares refinement. The temperature factors for all non-H atoms in the $-$COOH group are ~7. The oxidations have significant impact on the protein−substrate interaction, causing substantial conformational changes in the protein.

As illustrated in Figure 4c, the Cα traces of HPPK·HP·MgAMPCPP (*14*) and HPPK·HPO/HPO-1·MgAMPCPP (this paper) superimpose very well. The rmsd for all 158 pairs of Cα atoms is 0.12 Å. However, the presence of HPO, instead of HP, eliminates the hydrogen bond interaction between the carbonyl oxygen (acceptor) of L45 and the atom N8 (donor) of the pterin moiety (O−N distance = 2.91 Å, ref *14*) and causes the flip of the peptide bond between L45 and G46. Consequently, the amide group of G46 is now facing N8 of HPO; a water molecule comes in and bridges the interaction between the two atoms (Figure 5).

As shown in Figure 3b, HPO and HPO-1 molecules occupy the same binding site with an occupancy ratio of 0.50:0.50, and W89 has two conformations with an occupancy ratio of 0.50:0.50 as well. The HPO molecule with its electron density colored in green is associated with the W89 conformation with the green electron density map, which is identical to the HP/W89 relationship as observed in HPPK·HP·MgAMPCPP (*14*). The existence of HPO-1 with 50% occupancy gives rise to the second conformation of W89 also with 50% occupancy, which is similar to the HP-3/W89 relationship as observed in HPPK·HP-3·MgATP (*13*) and is illustrated in Figure 6. The conformational change of W89 is caused by its steric interaction with HP-3 in HPPK·HP-3·MgATP (*13*) and with HPO-1 in HPPK·HPO/HPO-1·MgAMPCPP (this paper). The bulky groups $-CH_3$ and $-CH_2-CH_2-C_6H_5$ at position 7 (Figure 1) cause not only the conformational change of W89 but also a significant conformational change of loop 3 (Figure 6), suggesting that the substitution of hydrogen atoms at position 7 by bulky groups may lower the binding affinity of the resulting compound toward the enzyme.

Mg^{2+} Binding in R92A. The asymmetric unit of R92A·Mg contains two independent protein molecules (A and B), three Mg^{2+} ions, three Cl^- ions, and 424 water molecules. Surprisingly, two Mg^{2+} ions are found coordinated with D95 and D97 in molecule B. However, the Mg^{2+} coordination is slightly different from that observed in the ternary complex HPPK·HP·MgAMPCPP (PDB 1eqo, ref *14*) (Figure 7). The two Mg^{2+}-coordination systems differ in the number of coordination water molecules and the nature of the additional negatively charged ligand. In the ternary complex, the negatively charged ligand is the phosphoryl chain of AMPCPP, whereas in R92A·Mg, it is the negatively charged side chain of E16 from molecule A (Figure 7). Three water molecules participate in Mg^{2+} coordination in the ternary complex, whereas six waters are found in R92A·Mg, among which two are conserved in both systems (Figure 7). The fact that the two Mg^{2+} ions in R92A·Mg are both coordinated with D95 and D97 as in the ternary complex HPPK·HP·MgAMPCPP suggests that D95 and D97 are well-positioned for the assembling of the catalytic center. However, it appears that only when an additional negatively charged ligand exists near D95 and D97, HPPK is able to form a stable complex with Mg^{2+} ions. To date, similar Mg^{2+} coordination has not been observed in any other apo-HPPK structures.

ACKNOWLEDGMENT

We would like to thank Drs. Z. Dauter and K. R. Rajashankar for their help during data collection and processing at the synchrotron beamline X9B of the NSLS, Brookhaven National Laboratory.

REFERENCES

1. Shiota, T. (1984) *Biosynthesis of folate from pterin precursors. Chemistry and Biochemistry of Folates*, John Wiley & Sons, New York.
2. Blakley, R. L., and Benkovic, S. J. (1984) in *Folates and Pterins* (Blakley, R. L., and Benkovic, S. J., Eds.), John Wiley & Sons, Inc., New York.
3. Cohen, M. L. (1992) *Science 257*, 1050−1055.
4. Neu, H. C. (1992) *Science 257*, 1064−1073.
5. Kunin, C. M. (1993) *Ann. Intern. Med. 118*, 557−561.
6. Levy, S. B. (1995) *Adv. Exp. Med. Biol. 390*, 1−13.
7. Murray, B. E. (1997) *Adv. Intern. Med. 42*, 339−367.
8. Hughes, D. T. D. (1997) *Sulphonamides. Antibiotic and Chemotherapy*, 7th ed., Churchill Livingstone, New York.
9. Hughes, D. T. D. (1997) in *Antibiotics and Chemotherapy* (O'Grady, F., Lambert, H. P., Finch, R. G., and Greenwood, D., Eds.) pp 346−356, Churchill Livingstone, New York.
10. Xiao, B., Shi, G., Chen, X., Yan, H., and Ji, X. (1999) *Structure Fold. Des. 7*, 489−496.
11. Hennig, M., Dale, G. E., D'Arcy, A., Danel, F., Fischer, S., Gray, C. P., Jolidon, S., Muller, F., Page, M. G., Pattison, P., and Oefner, C. (1999) *J. Mol. Biol. 287*, 211−219.
12. Xiao, B., Shi, G., Gao, J., Blaszczyk, J., Liu, Q., Ji, X., and Yan, H. (2001) *J. Biol. Chem. 276*, 40274−40281.
13. Stammers, D. K., Achari, A., Somers, D. O., Bryant, P. K., Rosemond, J., Scott, D. L., and Champness, J. N. (1999) *FEBS Lett. 456*, 49−53.
14. Blaszczyk, J., Shi, G., Yan, H., and Ji, X. (2000) *Structure Fold. Des. 8*, 1049−1058.
15. Shi, G., Blaszczyk, J., Ji, X., and Yan, H. (2001) *J. Med. Chem. 44*, 1364−1371.
16. Shi, G., Gao, J., and Yan, H. (1999) *J. Biomol. NMR 14*, 189−190.
17. Otwinowski, Z., and Minor, W. (1997) *Methods Enzymol. 276*, 307−326.
18. Navaza, J. (1994) *Acta Crystallogr. A 50*, 157−163.
19. Brünger, A. T. (1997) *Nature Struct. Biol. 4 Suppl.*, 862−865.
20. Sheldrick, G. M., and Schneider, T. R. (1997) *Methods Enzymol. 277*, 319−343.
21. Jones, T. A., and Kjeldgaard, M. (1997) *Methods Enzymol. 277*, 173−208.
22. Laskowski, R. A., MacArthur, M. W., Moss, D. S., and Thornton, J. M. (1993) *J. Appl. Crystallogr. 26*, 283−291.

BI0267994